Editors' Suggestion

Pauli energy contribution to the nucleus-nucleus interaction

A. S. Umar [1,*] C. Simenel [2,†] and K. Godbey [3,‡]

[1]*Department of Physics and Astronomy, Vanderbilt University, Nashville, Tennessee 37235, USA*

[2]*Department of Fundamental and Theoretical Physics and Department of Nuclear Physics and Accelerator Applications, Research School of Physics, Australian National University, Canberra ACT 2601, Australia*

[3]*Cyclotron Institute, Texas A&M University, College Station, Texas 77843, USA*

(Received 11 May 2021; accepted 4 August 2021; published 17 September 2021)

Background: The Pauli exclusion principle plays a crucial role as a building block of many-body quantal systems comprised of fermions. It also induces a "Pauli repulsion" in the interaction between di-nuclear systems. It has been shown in [Phys. Rev. C **95**, 031601(R) (2017)] that the Pauli repulsion widens the nucleus-nucleus potential barrier, thus hindering sub-barrier fusion.

Purpose: To investigate the proton and neutron contributions to the Pauli repulsion, both in the bare potential neglecting shape polarization and transfer between the reactants, as well as in the dynamical potential obtained by accounting for such dynamical rearrangements.

Methods: As the basis of our study we utilize the Pauli kinetic energy (PKE) obtained by studying the nuclear localization function (NLF). Recently this approach has been generalized to incorporate all of the dynamical and time-odd terms present in the nuclear energy density functional. This approach is employed in the density constrained frozen Hartree-Fock (DCFHF) and in the density constrained time-dependent Hartree-Fock (DC-TDHF) microscopic methods.

Results: The PKE spatial distribution shows that a repulsion occurs in the neck between the nuclei when they first touch. Inside the barrier, neutrons can contribute significantly more to the Pauli repulsion in neutron-rich systems. Dynamical effects tend to lower the Pauli repulsion near the barrier. Proton and neutron dynamical contributions to the PKE significantly differ inside the barrier for asymmetric collisions, which is interpreted as an effect of multinucleon transfer.

Conclusions: The PKE is shown to make a significant contribution to nuclear interaction potentials. Protons and neutrons can play very different roles in both the bare potential and in the dynamical rearrangement. Further microscopic studies are required to better understand the role of transfer and to investigate the effect of pairing and deformation.

DOI: 10.1103/PhysRevC.104.034619

I. INTRODUCTION

One of the most important features of quantum mechanics is the classification of particles based on their spin content as bosons and fermions. For quantum systems composed of fermions, the Pauli exclusion principle states that no two identical particles can occupy the same state. This principle, which was introduced by Pauli for electrons [1], was subsequently generalized to all fermions via the spin-statistics theorem [2,3]. For complex many-body systems, the Pauli principle manifests itself as a requirement that the wave function representing the system be antisymmetric under exchange of particles. In density functional theory (DFT) calculations for electronic systems, the construction of the so-called orbital-free DFT functionals contains a Pauli kinetic energy term in the energy decomposition. The orbital-based determination of the Pauli kinetic energy is found to be essential for gauging the accuracy of these empirical Pauli functionals [4,5]. Similarly, the identification of the contribution of Pauli repulsion in DFT calculations of intermolecular interaction energies is of current interest in chemistry [6–10].

Atomic nuclei, composed of neutrons and protons, must also adhere to the Pauli exclusion principle. This is strictly implemented in microscopic calculations of nuclear structure, primarily by adopting determinental many-body wave functions. Similar to intermolecular interactions, one expects, in the case of collisions of atomic nuclei, a Pauli repulsion induced by the Pauli exclusion principle between nucleons of different nuclei. Although this Pauli repulsion is often neglected in calculations of nucleus-nucleus potentials based on the observation that the overlap between collision partners at distances close to the fusion barrier radius is usually small, it has been shown that the Pauli repulsion can play a significant role in systems with large Z_1Z_2 (as more overlap is required to compensate the larger Coulomb repulsion), as well as at

*umar@compsci.cas.vanderbilt.edu

†cedric.simenel@anu.edu.au

‡Present address: Facility for Rare Isotope Beams, Michigan State University, East Lansing, Michigan 48824, USA; godbey@frib.msu.edu

energies well below the Coulomb barrier [11]. Indeed, in the latter case, fusion occurs via tunneling through a barrier widened by Pauli repulsion as the inner turning point corresponds to a substantial nuclear overlap with a more compact shape [12,13]. As a result, Pauli repulsion provides a natural, though partial, explanation to experimentally observed fusion hindrance at deep sub-barrier energies [14–16] (see Ref. [17] for a review). Note also that collisions well above the barrier are expected to be sensitive to Pauli repulsion as well [18–21].

Several techniques have been used in the past, with varying success, to incorporate the Pauli exclusion principle for the calculation of ion-ion potentials. These include techniques to orthogonalize overlapping nucleon wave functions [18,19], though the orthogonalization itself usually induces a spurious change of the density and thus of the nuclear attraction [11,22]. One approach is to replace the kinetic energy density using expressions based on the Thomas-Fermi approximation [23–25]. In this approach, however, the effect of other momentum-dependent terms as well as the spin-orbit interaction of the effective nucleon-nucleon interaction on the Pauli repulsion are not accounted for. A folding density method for α clusters has also been developed recently [26,27]. Attempts were made with the resonating group method [28–31] which, in principle, provides a theoretical approach to construct internuclear potentials with full antisymmetrization. However, such calculations have thus far been limited to light systems and direct reactions due to their complexity.

A natural way to describe heavy ion collisions, while accounting exactly for the Pauli exclusion principle, is to use microscopic theories in which the wave function of the entire system is a Slater determinant of nucleon wave functions (mean-field approximation) or a sum of such determinants (beyond mean-field approaches). In particular, the time-dependent Hartree-Fock (TDHF) theory, which describes the evolution of each particle in the self-consistent mean field produced by all particles, is appealing as it does not rely on a nucleus-nucleus potential. The validity of the mean-field approximation is based on the expectation that the Pauli principle plays an important role in simultaneously building up a time-dependent mean field and suppressing the propagation of the strong nucleon-nucleon interaction terms. Although the TDHF theory has been successful in describing various reaction mechanisms (see Refs. [32–35] for recent reviews), its main drawback is that it does not account for tunneling of the many-body wave function. Though imaginary-time mean-field methods are expected to overcome this limitation [36,37], only applications to simple systems have been achieved so far [38,39]. Therefore, descriptions of sub-barrier fusion nowadays are still based on calculations of barrier penetration with nucleus-nucleus potentials (see Refs. [17,40] for reviews).

It is possible to compute nucleus-nucleus potentials microscopically, using a single Slater determinant to describe the many-body wave function and account for Pauli repulsion. As an example, one can use the two-center shell model [41,42] or the constrained Hartree-Fock method [43]. However, both methods assume an adiabatic approximation. The latter, which is expected to hold in nuclear fission as it is a slow process, is questionable in the context of "faster" reactions such as fusion. For this reason, nucleus-nucleus potentials are more commonly computed with the frozen density approximation in which the nuclei are assumed to keep their ground-state densities. Fusion barriers can be computed with microscopically obtained nuclear densities by evaluating the interaction energy between the nuclei at an internuclear separation, R, while keeping these densities frozen [44]. Subsequently, the dynamics can be included via the coupled-channels approach [45]. Using this approximation with HF ground-state densities of the collision partners, one gets the frozen Hartree-Fock (FHF) method [43,46–50] which, completed with coupled-channel calculations to account for rearrangement of nuclear densities, provides a reasonable description of fusion at near-barrier energies [51]. FHF potentials, however, do not account for the Pauli repulsion as, at small R, it involves two overlapping Slater determinants (one per HF ground state). Thus, FHF potentials should not be used to describe fusion well below the barrier, or in systems with large Z_1Z_2 [11]. For this reason, we recently developed the so-called density-constrained frozen Hartree-Fock (DCFHF) method, which is based on the frozen density approximation, while describing the many-body system with a single Slater determinant, thus accounting for the Pauli exclusion principle exactly [11]. DCFHF is the static counterpart of the density constrained time-dependent Hartree-Fock (DC-TDHF) method which is used to determine nucleus-nucleus potentials including dynamical effects [52]. A comparison of FHF (static without Pauli repulsion), DCFHF (static with Pauli repulsion), and DC-TDHF (dynamics with Pauli repulsion) potentials thus provides valuable information on the respective roles of Pauli repulsion and dynamical density rearrangement. Nevertheless, the information one can access with this method is only global as we are dealing with quantities that are integrated over space. In order to get a deeper insight into the microscopic origin of Pauli repulsion, it is therefore desirable to express it in terms of a local quantity.

In this work, we achieve this using the nucleon localization function (NLF), which allows for a more precise characterization of the Pauli energy and in particular its spacial distribution. The electronic localization function (ELF) was originally developed in condensed matter physics [53–55] as a way to visualize the localized electronic groups in atomic and molecular systems [56]. The same idea was introduced to nuclear physics to bring out the clustering features of the nuclear densities obtained in mean-field calculations [57] and employed to bring out the cluster features of light nuclei [57,58], study of reactions [59], and shell effects in fission [60–64]. In a recent work, the NLF function was generalized to include all of the time-odd and spin-dependent terms of the Skyrme energy density functional [65]. As a by-product of these developments, we also have an accurate way to calculate the Pauli energy in a way similar to that employed in DFT calculations [4,5] for electronic systems while including all the nuclear energy density functional contributions.

We use the NLF approach to demonstrate the contribution of Pauli energy in nucleus-nucleus potentials calculated with the DCFHF and DC-TDHF methods. The NLF is expressed in terms of a Pauli localization function (PLF) to visualize these effects. In Sec. II, we give a brief outline of the

methods employed to compute the Pauli contribution to the ion-ion interaction barriers and we describe the Pauli energy calculations using the NLF. This is followed by the results of these calculations in Sec. III. Conclusions are summarized in Sec. IV.

II. METHOD

In this section, we briefly outline the formalisms and methods used in our calculations. Further details can be found in the cited references.

A. Microscopic methods

In order to investigate the Pauli energy in heavy-ion fusion reactions, we employ microscopic methods to compute the interaction between nuclei. Following the idea of Brueckner *et al.* [44], the bare nucleus-nucleus potential (i.e., without dynamical rearrangement) is computed from an energy density functional (EDF) $E[\rho]$ written as a space integral of an energy density $\mathcal{H}[\rho(\mathbf{r})]$

$$E[\rho] = \int d\mathbf{r}\ \mathcal{H}[\rho(\mathbf{r})]. \tag{1}$$

The bare potential is obtained by requiring frozen ground-state densities ρ_i of each nucleus ($i = 1, 2$), which we compute using the Hartree-Fock (HF) mean-field approximation. One advantage of this method is that it does not introduce new parameters other than those of the EDF. Indeed, the same Skyrme EDF [66] is used both in HF calculations and to compute the bare potential.

Neglecting the Pauli exclusion principle between nucleons in different nuclei (except for those arising from the exchange terms in the effective interaction [67]) leads to the usual FHF potential [43,46–50]

$$V_{\rm FHF}(\mathbf{R}) = \int d\mathbf{r}\ \mathcal{H}[\rho_1(\mathbf{r}) + \rho_2(\mathbf{r}-\mathbf{R})] - E[\rho_1] - E[\rho_2], \tag{2}$$

where $\mathbf{R}$ is the distance vector between the centers of mass of the nuclei. To account for the Pauli repulsion in the bare potential, we use instead the DCFHF method [11]. The Pauli exclusion principle is included exactly by allowing the single-particle states, constituting the combined nuclear density, to reorganize to attain their minimum energy configuration and be properly antisymmetrized, as the many-body state is a Slater determinant of all the occupied single-particle wave functions. The HF minimization of the combined system is thus performed subject to the constraint that the local proton (p) and neutron (n) densities do not change:

$$\delta\left\langle H - \sum_{q=p,n}\int d\mathbf{r}\ \lambda_q(\mathbf{r})\left[\rho_{1_q}(\mathbf{r}) + \rho_{2_q}(\mathbf{r}-\mathbf{R})\right]\right\rangle = 0, \tag{3}$$

where the $\lambda_{n,p}(\mathbf{r})$ are Lagrange parameters at each point of space constraining the neutron and proton local densities. This equation determines a unique Slater determinant $|\Phi(\mathbf{R})\rangle$. Assuming the potential to be central leads to the expression

$$V_{\rm DCFHF}(R) = \langle\Phi(\mathbf{R})|H|\Phi(\mathbf{R})\rangle - E[\rho_1] - E[\rho_2]. \tag{4}$$

The resulting DCFHF bare potentials thus account for the Pauli repulsion, widening the fusion barrier and producing a potential pocket at short distance R which is not present in FHF potentials [11]. Consequently, comparisons between FHF and DCFHF bare potentials allow us to study the effects of the Pauli principle for frozen nuclear densities. These potentials, however, do not account for any dynamical rearrangement of the densities induced.

TDHF calculations, on the other hand, account for such rearrangement, at the mean-field level, in particular those produced by couplings to vibrational [51,68,69] and rotational modes [70,71], as well as nucleon transfer through the neck [48,50,72–76]. Nucleus-nucleus potentials extracted from TDHF calculations [47,49,52,77] then account for both dynamical effects and the Pauli exclusion principle. In order to further investigate the full dynamics, we have thus used the DC-TDHF method, where the densities are taken directly from the TDHF evolution of the system and the same constraint procedure used in DCFHF is employed (see Ref. [52] for details):

$$\delta\left\langle H - \sum_{q=p,n}\int d\mathbf{r}\ \lambda_q(\mathbf{r})[\rho_q(\mathbf{r}) - \rho_q^{\rm TDHF}(\mathbf{r},t)]\right\rangle = 0,$$

where ρ_q represents the combined density for the system. The TDHF evolution gives access to the time evolution of the distance $R(t)$ between the centers of mass of the fragments. The potential is then obtained as in Eq. (2) by removing the binding energy of the HF ground states,

$$V_{\text{DC-TDHF}}(R) = \langle\Phi(\mathbf{R}(\mathbf{t}))|H|\Phi(\mathbf{R}(\mathbf{t}))\rangle - E[\rho_1] - E[\rho_2]. \tag{5}$$

The DC-TDHF approach accounts for microscopic effects associated with the Pauli exclusion principle, such as the splitting of orbitals with some states contributing attractively (bounding) and some repulsively (antibounding) to the potential [78]. It should be noted also that, due to their dynamical nature, density rearrangements naturally depend on the energy of the collision, inducing an energy dependence to the potential [47,79–81]. One limitation of methods relying on TDHF evolutions is that the latter do not account for many-body tunneling. Thus, the energy dependence of the potential at sub-barrier energies is unknown. Nevertheless, near- and sub-barrier fusion cross sections have been computed using DC-TDHF potentials determined from TDHF evolutions at near-barrier central collisions, showing overall good agreement with experiment [69,81–88].

B. The nucleon localization function (NLF)

The measure of localization has been originally developed in the context of a mean-field description for electronic systems [53–55] and subsequently introduced to nuclear systems [57,65]. We first realize that a fermionic mean-field state is fully characterized by the one-body density-matrix $\rho_q(\mathbf{r}s, \mathbf{r}'s')$. The probability of finding two nucleons with the same spin at spatial locations $\mathbf{r}$ and $\mathbf{r}'$ (same-spin pair probability) for isospin q is proportional to

$$P_{qs}(\mathbf{r},\mathbf{r}') = \rho_q(\mathbf{r}s,\mathbf{r}s)\rho_q(\mathbf{r}'s,\mathbf{r}'s) - |\rho_q(\mathbf{r}s,\mathbf{r}'s)|^2, \tag{6}$$

which vanishes for $\mathbf{r} = \mathbf{r}'$ due to the Pauli exclusion principle. The conditional probability for finding a nucleon at $\mathbf{r}'$ when we know with certainty that another nucleon with the same spin and isospin is at $\mathbf{r}$ is proportional to

$$R_{qs}(\mathbf{r}, \mathbf{r}') = \frac{P_{qs}(\mathbf{r}, \mathbf{r}')}{\rho_q(\mathbf{r}s, \mathbf{r}s)}. \tag{7}$$

The short-range behavior of R_{qs} can be obtained using techniques similar to the local density approximation [57,65]. The leading term in the expansion yields the localization measure

$$D_{qs_\mu} = \tau_{qs_\mu} - \frac{1}{4}\frac{|\nabla \rho_{qs_\mu}|^2}{\rho_{qs_\mu}} - \frac{|\mathbf{j}_{qs_\mu}|^2}{\rho_{qs_\mu}}. \tag{8}$$

This measure is the most general form that is appropriate for deformed nuclei and without assuming time-reversal invariance, thus also including the time-odd terms important in applications such as cranking or TDHF. The densities and currents are given in their most unrestricted form [89–91] for μ axis denoting the spin-quantization axis by [65]

$$\rho_{qs_\mu}(\mathbf{r}) = \tfrac{1}{2}\rho_q(\mathbf{r}) + \tfrac{1}{2}\sigma_\mu s_{q\mu}(\mathbf{r}), \tag{9a}$$

$$\tau_{qs_\mu}(\mathbf{r}) = \tfrac{1}{2}\tau_q(\mathbf{r}) + \tfrac{1}{2}\sigma_\mu T_{q\mu}(\mathbf{r}), \tag{9b}$$

$$\mathbf{j}_{qs_\mu}(\mathbf{r}) = \tfrac{1}{2}\mathbf{j}_q(\mathbf{r}) + \tfrac{1}{2}\sigma_\mu \mathbb{J}_q(\mathbf{r}) \cdot \mathbf{e}_\mu, \tag{9c}$$

where $\sigma_\mu = 2s_\mu = \pm 1$ and $\mathbf{e}_\mu$ is the unit vector in the direction of the μ axis. Note that subscripts s_μ denote spin along the quantization axis and should not be confused by the spin density $s_{q\mu}$. The dot product in Eq. (9) is explicitly given in the case of, e.g., $\mu = z$:

$$\mathbb{J}_q(\mathbf{r}) \cdot \mathbf{e}_z = \frac{1}{2i}[(\nabla - \nabla')s_{qz}(\mathbf{r}, \mathbf{r}')]_{\mathbf{r}=\mathbf{r}'}.$$

The explicit expressions of the local densities and currents are given in Refs. [65,89]. We note that the localization measure includes the spin density $s_{q\mu}(\mathbf{r})$, the time-odd part of the kinetic density $T_{q\mu}(\mathbf{r})$, as well as the full spin-orbit tensor $\mathbb{J}_q(\mathbf{r})$, which is a pseudotensor. In this sense, all of the terms in the Skyrme energy density functional [89] contribute to the measure. Finally, we note that the time-odd terms contained in the above definitions ($s_{q\mu}$, $T_{q\mu}$, and $\mathbf{j}_q$) are zero in static calculations of even-even nuclei but the spin tensor $\mathbb{J}_q$ is not. Therefore, $\mathbf{j}_{qs_\mu}$ is not zero in general. The DCFHF and DC-TDHF procedures result in a time-reversal invariant solution where the time-odd terms are zero. However, all time-odd terms are present in TDHF calculations as they assure Galilean invariance of the time evolution. Thus, the TDHF densities used in the DC-TDHF method are generated with the presence of time-odd terms, resulting in an excitation energy that is removed by the DC-TDHF procedure [79].

An alternate meaning of the localization function relates to the kinetic energy and the Pauli exclusion principle. In fact, the last two terms in Eq. (8) are the kinetic density for a complex valued single particle state of a given spin s and isospin q that satisfies local gauge invariance [65,92]

$$\tau^{\text{s.p.}}_{qs} = \frac{1}{4}\frac{|\nabla \rho_{qs}|^2}{\rho_{qs}} + \frac{|\mathbf{j}_{qs}|^2}{\rho_{qs}}. \tag{10}$$

The first term in Eq. (10) is related to the von Weizsacker kinetic-energy density [93]. Equations (8) and (10) give

$$D_{qs} = \tau_{qs} - \tau^{\text{s.p.}}_{qs}, \tag{11}$$

meaning that, for a single nucleon system, $D_{qs} = 0$. Consequently, D_{qs} is a measure of the excess of kinetic density due to the Pauli exclusion principle. One can now define the Pauli kinetic energy (PKE) from the above expression as

$$E^{\text{P}}_{qs} = \frac{\hbar^2}{2m}\int d^3r\, D_{qs}(\mathbf{r}). \tag{12}$$

Note that this is the intrinsic PKE produced by all nucleons of any nuclear system. So far, these equations are general and can be used to compute the PKE from different mean-field approaches by using the corresponding one-body density matrix.

For example, using a DCFHF one-body density matrix $\rho^{\text{DCFHF}}(R)$ for nuclei at a distance R in Eq. (8), one can compute the total PKE with Eq. (12) from the resulting $D^{\text{DCFHF}}_{qs}(R; \mathbf{r})$. However, the Pauli exclusion principle between nucleons belonging to the same nucleus do not contribute to the Pauli repulsion in the nucleus-nucleus potential. We then define the net PKE for two nuclei separated by a distance R between their centers as

$$\Delta E^{\text{P(F)}}_{q\mu}(R) = \frac{\hbar^2}{2m}\sum_{s_\mu}\int d^3r\, \left[D^{\text{DCFHF}}_{qs_\mu}(\mathbf{r}, R) - D^{\text{FHF}}_{qs_\mu}(\mathbf{r}, R)\right], \tag{13}$$

where we have subtracted the contribution of the PKE from the FHF approach. Indeed, the latter uses the same frozen density as DCFHF, but it neglects the Pauli exclusion principle between nucleons of different nuclei. We have also summed over the spin-up and spin-down components for a given spin projection axis μ. The notation P(F) stands for "Pauli in the frozen approximation."

The calculation of this PKE difference with frozen densities allows one to identify the internuclear PKE without the presence of particle transfer and other relaxation effects similar to methods used in condensed matter physics and chemistry [6,7,9]. We note that $\Delta E^{\text{P(F)}}(R)$ is zero for large values of R since the antisymmetrization of two well-separated nuclei does not introduce any change to local nuclear densities of Eq. (9) and thus both DCFHF and FHF give the intrinsic Pauli energy in this case. We note also that, assuming that the PKE is independent of the choice of the spin quantization axis, summing over the isospin q gives the total Pauli repulsion which should then be equivalent to the difference between the DCFHF and FHF potentials, $\sum_q \Delta E^{\text{P(F)}}_{q\mu}(R) \simeq V_{\text{DCFHF}}(R) - V_{\text{FHF}}(R)$.

We can similarly define the dynamical contribution to this net PKE by taking the difference between the DC-TDHF and DCFHF localization measures

$$\Delta E^{\text{P(D)}}_{q\mu}(R) = \frac{\hbar^2}{2m}\sum_{s_\mu}\int d^3r \times \left[D^{\text{DC-TDHF}}_{qs_\mu}(\mathbf{r}, R) - D^{\text{DCFHF}}_{qs_\mu}(\mathbf{r}, R)\right], \tag{14}$$

where (D) stands for "dynamical contribution." In this way, we can easily compare the static (i.e., in the frozen approximation) and dynamical contributions to the Pauli repulsion.

It is interesting to visualize the NLF as it is also defined from the localization measure in Eq. (8). We first normalize the localization measure using [4,65]

$$\mathcal{D}_{qs_\mu}(\mathbf{r}) = \frac{D_{qs_\mu}(\mathbf{r})}{\tau^{\rm TF}_{qs_\mu}(\mathbf{r})}, \tag{15}$$

where the normalization $\tau^{\rm TF}_{qs_\mu}(\mathbf{r}) = \frac{3}{5}(6\pi^2)^{2/3}\rho^{5/3}_{qs_\mu}(\mathbf{r})$ is the Thomas-Fermi kinetic density. The NLF can then be represented either by $1/\mathcal{D}_{qs_\mu}$ or by

$$C_{qs_\mu}(\mathbf{r}) = \left[1 + \mathcal{D}^2_{qs_\mu}\right]^{-1}. \tag{16}$$

The advantage of the latter form is that it scales to be in the interval [0,1], but otherwise both forms show similar localization details. We also see that while this is called the NLF, it is a visual measure of the Pauli energy.

C. Numerical details

Calculations were done in a three-dimensional Cartesian geometry with no symmetry assumptions using the code of Ref. [94] and using the Skyrme SLy4d interaction [95], which has been successful in describing various types of nuclear reactions [32,33]. The three-dimensional Poisson equation for the Coulomb potential is solved by using fast-Fourier transform techniques and the Slater approximation is used for the Coulomb exchange term. The static HF equations and the DCFHF minimizations are implemented using the damped gradient iteration method [96]. The box size used for all the calculations was chosen to be $60 \times 30 \times 30$ fm^3, with a mesh spacing of 1.0 fm in all directions. These values provide very accurate results due to the employment of sophisticated discretization techniques [97,98].

III. RESULTS

A. NLF and Pauli energy distribution

The outcome of a central heavy-ion collision at near barrier energy is highly sensitive to the structure and dynamics of the system at the barrier radius R_B, i.e., when short-range nuclear attraction and long-range Coulomb repulsion compensate. The proton and neutron frozen densities in ^{48}Ca + ^{48}Ca and ^{16}O + ^{208}Pb are represented in Figs. 1(a) and 1(b) and Figs. 2(a) and 2(b), respectively. In both cases, the neck density is small and does not exceed 20% of the saturation density. Note, however, that R_B is determined from DC-TDHF potentials including shape polarization, which may slightly increase the neck density. Nevertheless, one would expect that the small neck density in the frozen calculations implies that the Pauli repulsion should remain small *a priori*. This expectation, however, is based on the assumption that the nucleons contributing to the neck density are essentially localized in the neck.

To verify this assumption, we plot the normalized NLF from DCFHF using Eq. (16) in Figs. 1(c), 1(d), 2(c), and 2(d). Interestingly, while the densities of the fragments add up in the neck region, the NLF behave differently with an apparent repulsion flattening the facing surfaces of the NLF near contact. A possible interpretation is that the neck nucleons could be delocalized, i.e., belonging to both fragments. This would provide a microscopic support to the "collectivization" mechanism invoked by Zagrebaev [99]. However, this observation, in itself, does not necessarily imply a large Pauli repulsion. Nevertheless, it weakens the validity of the commonly used

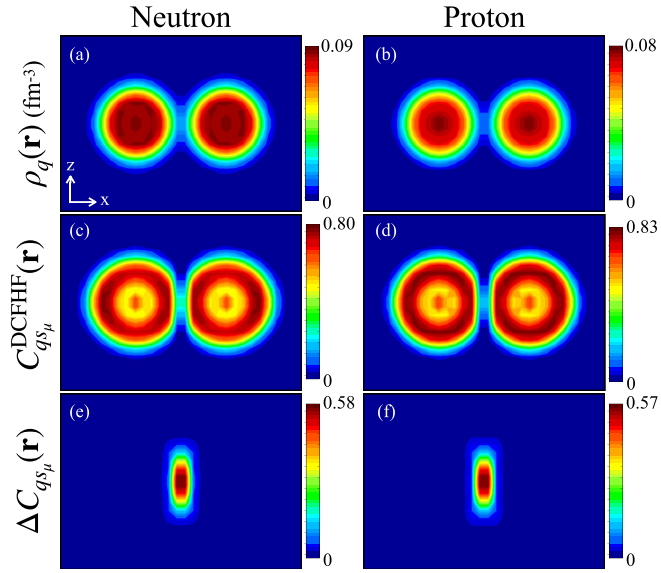

FIG. 1. Frozen neutron (a) and proton (b) HF densities in ^{48}Ca + ^{48}Ca for a distance between the nuclei close to the barrier radius $R_B \simeq 10.8$ fm. Only a subpart of the numerical box is shown, with 29×21 fm^2 in the (x, z) plane. Corresponding normalized NLF, computed from Eq. (16) for spin up (along the $\mu = z$ axis) with the DCFHF method, are plotted in panels (c) and (d). (The plots for spin down are similar). The difference $\Delta C_{qs_z} = C^{\rm FHF}_{qs_z} - C^{\rm DCFHF}_{qs_z}$ between FHF and DCFHF normalized NLF are plotted in panels (e) and (f).

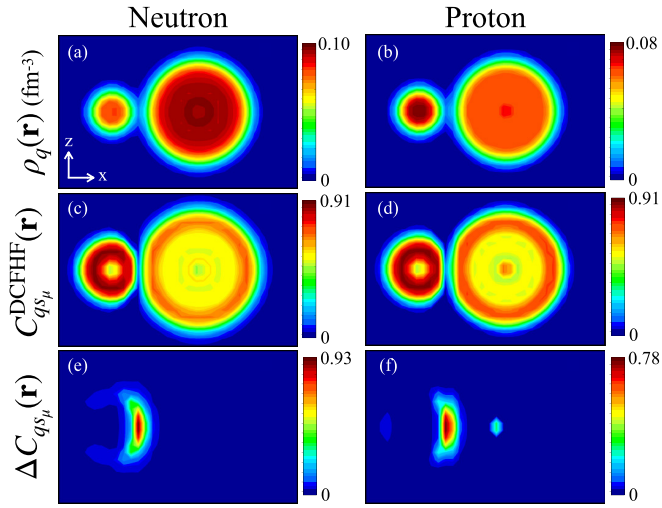

FIG. 2. Same as Fig. 1 for ^{16}O + ^{208}Pb with $R_B \simeq 12$ fm. The part of the box that is represented covers 33×21 fm^2 in the (x, z) plane.

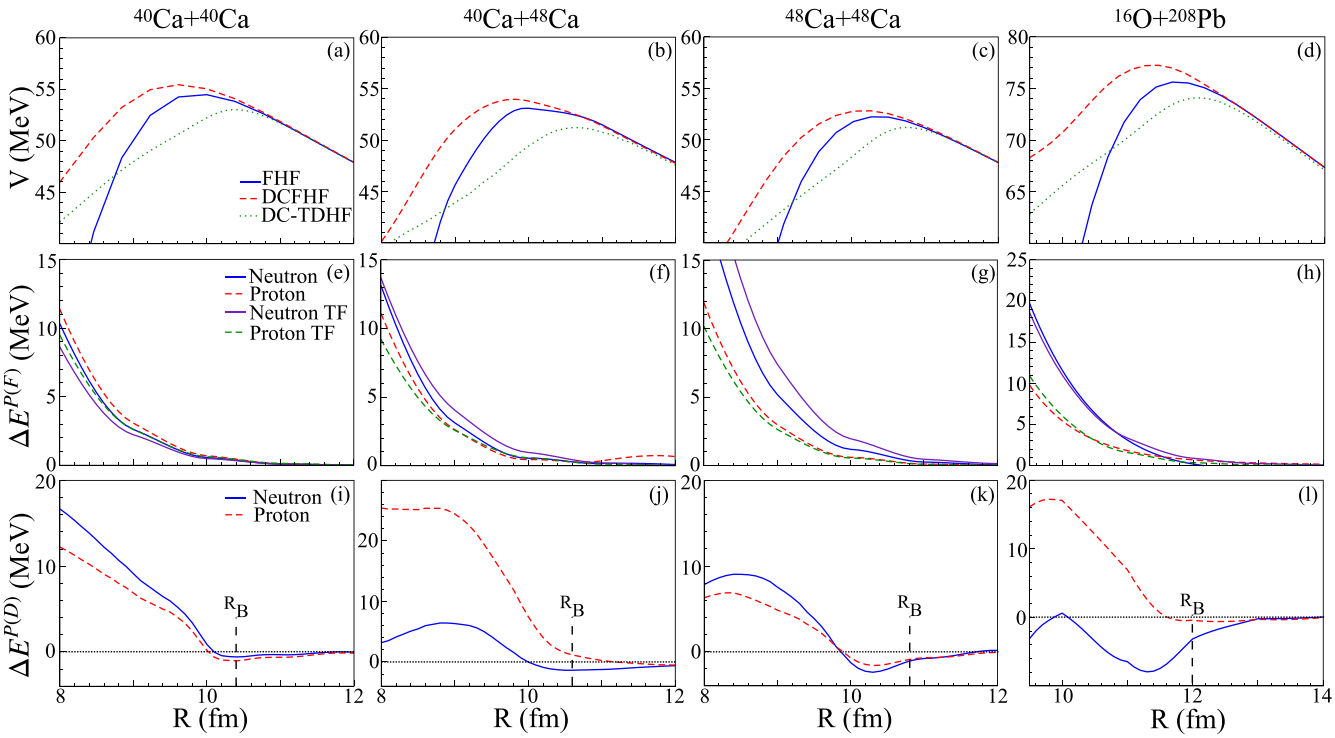

FIG. 3. [(a)–(d)] Nucleus-nucleus potentials in ^{40,48}Ca + ^{40,48}Ca and ^{16}O + ^{208}Pb computed from FHF, DCFHF, and DC-TDHF methods. [(e)–(h)] Neutron and proton contributions to the Pauli repulsion from Eq. (13) in the frozen approximation (thick lines). Replacing the DCFHF Pauli energy by the FHF one with Thomas-Fermi approximation of the kinetic energy in Eq. (13) leads to results represented by thin lines. [(i)–(l)] Additional dynamical contributions to the Pauli repulsion computed from Eq. (14). The line marked by R_B indicates the (DC-TDHF) barrier peak for each system. The dotted horizontal lines show the location of zero PKE difference.

assumption that Pauli repulsion can be neglected when the density in the neck is small compared to saturation density.

To get a deeper insight into the spatial distribution of the Pauli repulsion, we plot the difference of the NLF computed from FHF and DCFHF in Figs. 1(e), 1(f), 2(e), and 2(f). As expected, this difference is mostly found around the neck region as it is due to the symmetrization process which tends to delocalize the neck nucleons. As a result, the Pauli repulsion is mostly occurring in the neck region. Note, however, that in the asymmetric ^{16}O + ^{208}Pb reaction, the spatial distribution of the Pauli repulsion also extends away from the neck. This distribution is also found be different for neutrons and protons. Quantitative comparisons between neutron and proton repulsion are discussed in the next section.

B. Pauli repulsion from potentials and NLF

Pauli repulsion is a contribution to the bare nucleus-nucleus potential which becomes important at short distance when the nuclei overlap. The FHF and DCFHF potentials are represented by solid and dashed lines, respectively, in Figs. 3(a)–3(d) for the ^{40,48}Ca + ^{40,48}Ca and ^{16}O + ^{208}Pb systems. The Pauli repulsion included in DCFHF induces a widening of the barrier as well as a small increase of its height, up to ≈1.6 MeV in ^{16}O + ^{208}Pb. To a large extent, this increase of the barrier height is compensated by dynamical polarization effects accounted for in the DC-TDHF potential [dotted lines in Fig. 3(a)–3(d)]. Indeed, coupling effects in these systems lower the average DC-TDHF barrier by few MeV. Nevertheless, the widening of the barrier due to Pauli repulsion is still present, indicating that it plays an important role in the inner barrier region.

The NLF method allows us to decompose the Pauli repulsion into proton and neutron contributions. This decomposition would make sense, however, only if the resulting Pauli energy does not strongly depend on the choice of the spin quantization axis μ in the region of interest. This dependence is studied in Fig. 4 for ^{40}Ca + ^{40}Ca by comparing $\mu = z$ and x spin quantization axes. Although the difference reaches ≈10% at very short distances, it remains small in the region studied in Fig. 3, which is physically relevant for sub-barrier fusion reactions down to ≈20% below the barrier. We have chosen the spin projection axis to be the z axis (perpendicular to the collision axis x) in all the following calculations. In general, except at small distances (where the frozen density distributions become unphysical), we do not see any significant dependence on the choice of the spin projection axis.

Before we study in more detail the proton and neutron contributions to the Pauli repulsion, we need to verify that the NLF method gives the expected Pauli repulsion. A comparison between Pauli repulsion calculations from the potential difference $V^{\rm DCFHF} - V^{\rm FHF}$ and using the NLF method in the frozen approximation [Eq. (13)] is shown in Fig. 5 for ^{40}Ca + ^{40}Ca. The overall agreement between both methods is good, although the NLF method slightly overestimates the Pauli repulsion in the barrier region (see inset of Fig. 5). It

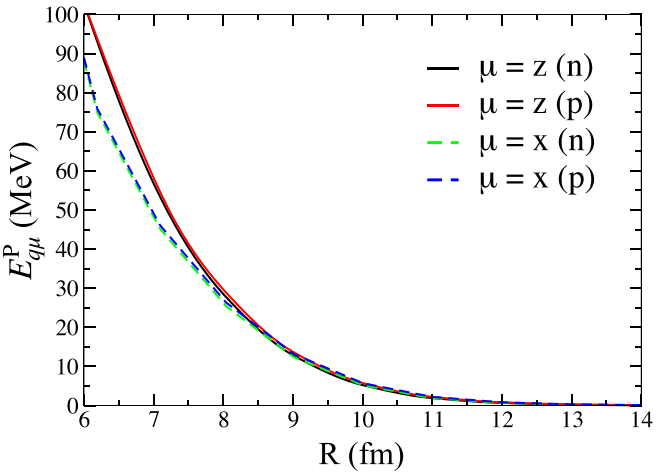

FIG. 4. Proton and neutron Pauli energy in ^{40}Ca + ^{40}Ca computed from DCFHF using Eq. (12) and summing over spin, $E^{P}_{q\mu} = \sum_{s_\mu} E^{P}_{qs_\mu}$. The solid and dashed lines are obtained with the quantization axis $\mu = z$ and x, respectively.

should be noted, however, that the localization measure in Eq. (8) is obtained within the local density approximation and that higher order terms in the expansion may account for this difference. Nevertheless, the calculated difference is small enough so that we can now turn our attention to investigating proton and neutron contributions to the Pauli repulsion with the NLF method.

C. Proton and neutron contributions to Pauli repulsion

Proton and neutron contributions to the Pauli repulsion, computed from Eq. (13) in the frozen approximation, are shown in Figs. 3(e)–3(h). All systems exhibit a sharp rise of Pauli repulsion inside the barrier. In all systems, the PKE acquires substantial values for small ion-ion separations (see also Fig. 5 for ^{40}Ca + ^{40}Ca where the Pauli repulsion keeps increasing inside the barrier). This is the root of the development of a potential pocket at short distances as the contribution from the PKE must overcome the sharp decline of the frozen density FHF potentials.

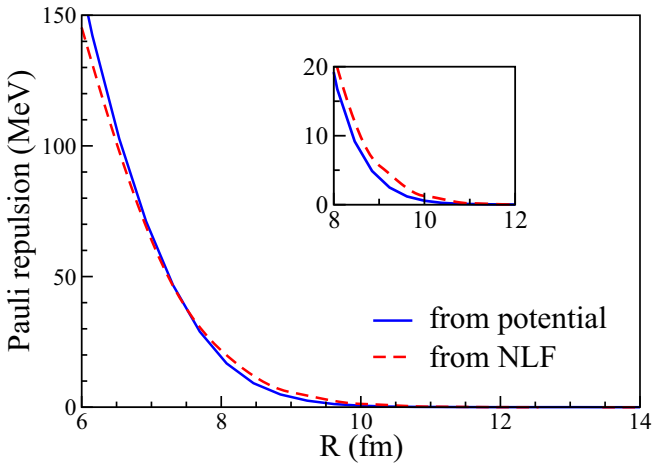

FIG. 5. Pauli repulsion in ^{40}Ca + ^{40}Ca. The solid line is obtained from the potential difference $V^{DCFHF} - V^{FHF}$. The dashed line is the sum of neutron and proton net PKE from Eq. (13) with $\mu = z$ spin quantization axis. The inset shows the same quantities in the barrier region.

Both proton and neutron contributions remain very close in the $N = Z$ system ^{40}Ca + ^{40}Ca. Although the proton contribution remains almost unchanged in all ^{40,48}Ca + ^{40,48}Ca systems, the Pauli repulsion significantly increases with the number of neutrons inside the barrier. For instance, at $R \simeq 9$ fm in ^{48}Ca + ^{48}Ca, which corresponds approximately to the inner turning point of a tunneling path at $\approx 0.9 V_B$ through the bare potential, the Pauli repulsion is still largely dominated by neutrons, with $\Delta E^{P(F)}_{pz}(9\text{ fm}) \simeq 3$ MeV and $\Delta E^{P(F)}_{nz}(9\text{ fm}) \simeq 5$ MeV. As a result, the ratio of the neutron contribution to the proton one largely exceeds the neutron-to-proton ratio. A similar behavior is observed in ^{16}O + ^{208}Pb, where the neutron contribution is about twice that of protons inside the barrier. This can be interpreted as an effect of neutron skins which develop in neutron rich nuclei and which make the neutrons "touch first" near the barrier radius. The Pauli exclusion principle acts then first on neutrons in such systems. Consequently, one may expect a fusion hindrance due to the Pauli exclusion principle in neutron-rich systems, in particular at sub-barrier energies.

We finally note that, in the asymmetric systems ^{40}Ca + ^{48}Ca and ^{16}O + ^{208}Pb, the proton contribution exceeds the neutron one at large distance, i.e., at $R > R_B$. The origin of this behavior is not clear. Note that it is not captured by the Thomas-Fermi approximation (see Sec. III D). We saw in Sec. III A that the Pauli exclusion principle tends to delocalize the neck nucleons. It is possible that this delocalization cost more energy for protons than neutrons, in particular in asymmetric systems.

D. Test of the Thomas-Fermi approximation

It has been suggested by several groups [19,24,25] that, when constructing ion-ion potentials using frozen densities, the Pauli kinetic energy induced by antisymmetrization could be approximated by replacing the kinetic density by the Thomas-Fermi expression

$$\tau^{TF}_{qs_\mu}(\mathbf{r}) = \tfrac{3}{5}(6\pi^2)^{2/3}\rho^{5/3}_{qs_\mu}(\mathbf{r}).$$

We have tested this approach by replacing $D^{DCFHF}_{qs_\mu}(\mathbf{r}, R)$ in Eq. (13) with the FHF expression evaluated with the Thomas-Fermi kinetic density. The results are plotted in Figs. 3(e)–2(h) with thin lines.

Overall, the Thomas-Fermi approximation provides results in good agreement with the NLF method. In particular, it underestimates the NLF calculation in ^{40}Ca + ^{40}Ca by less than 1 MeV (except at $R \approx 8$ fm). The agreement is also good at short distance in ^{16}O + ^{208}Pb. Near the barrier, however, the Thomas-Fermi approximation overestimates the neutron contribution by about 1 MeV in this system. As a result, it does not reproduce the dominant proton contribution at the barrier, which is predicted by the NLF method in both ^{16}O + ^{208}Pb and ^{40}Ca + ^{48}Ca. Another observation is that, in reactions with ^{48}Ca, the splitting between neutron and proton contri-

butions to the Pauli repulsion is somewhat overestimated by the Thomas-Fermi approximation.

We conclude that, though the Thomas-Fermi approximation gives a reasonably good estimate of the Pauli repulsion, it does not always reproduce the various features of the proton and neutron contributions. In fact, in using the Thomas-Fermi approximation, one implicitly assumes that the Pauli repulsion only affects the kinetic density, while in fact it also has an impact on other terms such as the spin-orbit contribution to the energy [11]. It should also be noted that we only consider doubly magic spherical nuclei which do not have pairing contributions at the mean-field level. Therefore, it would be interesting to test the Thomas-Fermi approximation in mid-shell nuclei as well. This will be the purpose of a future work.

E. Effect of dynamical rearrangement on Pauli energy

As long as we are dealing with frozen densities, the DCFHF method embodies the aspects of antisymmmetrization to produce an optimum prediction of the PKE at the (static) mean-field level. However, in a more realistic dynamical description of the reaction, the densities of the collision partners are no longer frozen but start to interact with one another even before the barrier peak, resulting in a shape polarization and possible transfer of nucleons between the fragments. Naturally, these processes occur while also maintaining the Pauli principle. In the context of DFT, such dynamics are described by the TDHF (or TDDFT) evolution. In the DC-TDHF methods, the nucleus-nucleus potential is determined from such time-dependent densities. A comparison between Pauli repulsion computed with the frozen approximation and with DC-TDHF will then provide a deeper insight into the dynamical rearrangement of the Pauli kinetic energy.

Figures 3(i)–3(l) show the difference in Pauli energies calculated using DC-TDHF and DCFHF methods as a function of the internuclear distance R. In all systems, the total Pauli repulsion (summed over proton and neutron contributions) is reduced near the barrier radius R_B once dynamics is included. As TDHF equations are obtained from a stationary action principle (usually leading to a minimum action), and because the PKE increases the action, it is natural for the system to explore paths in which the density is rearranged to reduce the PKE. At shorter distances, however, an increase of the total PKE is observed. It should be noted that the density distributions obtained at small R are usually very different to the frozen densities and that the difference of PKE at $R < R_B$ may not be always meaningful. Nevertheless, the observed increase of Pauli repulsion due to dynamics at short distance could also have a physical origin, such as a dynamical collectivization of the nucleons (increasing the PKE) when the collision partners merge into a single system.

We now turn our attention to the difference between proton and neutron contributions to the dynamical rearrangement of the net PKE in Figs. 3(i)–3(l). Both species behave similarly in the symmetric ^{40}Ca + ^{40}Ca and ^{48}Ca + ^{48}Ca reactions, though in both cases neutrons induce a slightly stronger repulsive dynamical contribution at short distance. In the asymmetric ^{40}Ca + ^{48}Ca and ^{16}O + ^{208}Pb systems, however, the dynamics induce a strong net PKE for the protons, while the neutron contribution remains small, and even attractive in the ^{16}O + ^{208}Pb system. In terms of dynamics, the main difference between the symmetric and asymmetric collisions is the opening of transfer channels in the latter, driven by an N/Z equilibration between the nuclei. This is a rapid process, with a timescale of the order of 1 zs [100], that occurs as soon as the nuclei are in contact. In both reactions, we expect a (multi)proton transfer from the light ($N = Z$) to the heavy ($N > Z$) nucleus, while neutrons are expected to flow the other way, as demonstrated in experimental studies of ^{16}O + ^{208}Pb [101,102]. In both reactions, the Pauli exclusion principle prevents protons to be transferred to similar states as they are already occupied. This could be a possible explanation for the increase of the net PKE due to proton dynamics. On the other hand, neutrons can be transferred to unoccupied final states with similar structure to the initial state. In this case, the Pauli exclusion principle is not "opposed" to the transfer and no particular rise of the PKE is expected. This simple interpretation could be tested with TDHF through a microscopic analysis of the initial and final states involved in the transfer (see, e.g., Fig. 22 of Ref. [33]). Such tests will be the subject of future work.

IV. CONCLUSIONS

The impact of the Pauli exclusion principle on various models and approaches of calculating the interaction of two nuclei has been a topic of interest for a long time. This is mainly predicated by the fact that, in most approaches, the influence of antisymmetrization has been an afterthought. Furthermore it has been argued that such effects are minimal at the barrier peak. Naturally, this was first found to be not true in α-nucleus potentials and subsequently at higher bombarding energies and for deep sub-barrier energies. Various remedies included the simple antisymmetrization of states between the two nuclei, which was found to require a normalization factor since the resulting states do not necessarily represent the lowest energy configuration, or the phenomenological shallow potential approach that introduced empirically adjusted potential pockets [103].

The recently proposed DCFHF method has been employed to compute bare nucleus-nucleus potentials in ^{40,48}Ca + ^{40,48}Ca and ^{16}O + ^{208}Pb reactions. This method not only does the necessary antisymmmetrization but also minimizes the energy of the system by keeping the density frozen but adjusting the underlying orbitals. In addition to accounting for the Pauli exclusion principle exactly (at the mean-field level), an appealing aspect of this method is that it does not require additional parameters other than those of the Skyrme EDF used to build the nuclear mean-field. By comparison with the more standard FHF (which neglects the Pauli exclusion principle between nucleons of different nuclei), we can compute the Pauli repulsion between the nuclei, which essentially widens the barrier and increases its height, thus hindering sub-barrier fusion.

We have employed the Pauli kinetic energy expression that arises from the study of the nuclear localization function within the realm of the density functional theory.

The spatial distribution of the Pauli kinetic energy shows that the repulsion occurs essentially in the neck between the fragments when the latter are at a distance equivalent to the barrier radius. The Pauli kinetic energy has also been used to decompose the Pauli repulsion into its proton and neutron contributions, We have shown that, inside the barrier, the contribution due to neutron dominates in neutron-rich systems, which is expected to further hinder sub-barrier fusion in such systems.

Additional effects due to the dynamics of the Pauli kinetic energy have been studied with the DC-TDHF method. We showed that, near the barrier, the system is usually able to find a path that reduces the Pauli repulsion. Inside the barrier, however, the net effect of the dynamics is essentially to increase the Pauli kinetic energy when the nuclei merge and the nucleons are subject to a collectivization process. A strong difference between proton and neutron dynamical contributions to the PKE is observed in the asymmetric systems we have studied. It is interpreted as an effect of multinucleon transfer induced by a rapid N/Z equilibration. Note that the availability of several states following transfer with positive Q values could counterbalance the Pauli repulsion that, in general, is predicted to reduce tunneling probability inside the Coulomb barrier [104,105].

Future directions include the study of Pauli repulsion in midshell nuclei to investigate the effects of pairing and deformation. In addition, it would be interesting to get a deeper insight into the interplay between transfer and Pauli kinetic energy through microscopic analysis of single-particle states involved in the transfer mechanism.

ACKNOWLEDGMENTS

We thank W. Nazarewicz for useful discussions. This work has been supported by the U.S. Department of Energy under Grant No. DE-SC0013847 with Vanderbilt University and by NNSA Cooperative Agreement No. DE-NA0003841, and by the Australian Research Councils Grant No. DP190100256.

[1] W. Pauli, Über Den Zusammenhang Des Abschlusses Der Elektronengruppen im atom mit der komplexstruktur der spektren, Z. Phys. **31**, 765 (1925).
[2] M. Fierz, Über die relativistische Theorie kräftefreier Teilchen mit beliebigem Spin, Helv. Phys. Acta **12**, 3 (1939).
[3] W. Pauli, The connection between spin and statistics, Phys. Rev. **58**, 716 (1940).
[4] S. Liu, D. Zhao, C. Rong, T. Lu, and S. Liu, Using Pauli energy to appraise the quality of approximate semilocal noninteracting kinetic energy density functionals, J. Chem. Phys. **150**, 204106 (2019).
[5] B. Patra, S. Jana, L. A. Constantin, and P. Samal, Relevance of the Pauli kinetic energy density for semilocal functionals, Phys. Rev. B **100**, 155140 (2019).
[6] Q. Wu, P. W. Ayers, and Y. Zhang, Density-based energy decomposition analysis for intermolecular interactions with variationally determined intermediate state energies, J. Chem. Phys. **131**, 164112 (2009).
[7] M. Raupach and R. Tonner, A periodic energy decomposition analysis method for the investigation of chemical bonding in extended systems, J. Chem. Phys. **142**, 194105 (2015).
[8] A. Sarsa, J. M. Alcaraz-Pelegrina, and C. Le Sech, Exclusion principle repulsion effects on the covalent bond beyond the Born-Oppenheimer approximation, Phys. Chem. Chem. Phys. **21**, 10411 (2019).
[9] D. M. Andrada and C. Foroutan-Nejad, Energy components in energy decomposition analysis (EDA) are path functions: Why does it matter? Phys. Chem. Chem. Phys. **22**, 22459 (2020).
[10] P. R. Horn, Y. Mao, and M. Head-Gordon, Defining the contributions of permanent electrostatics, Pauli repulsion, and dispersion in density functional theory calculations of intermolecular interaction energies, J. Chem. Phys. **144**, 114107 (2016).
[11] C. Simenel, A. S. Umar, K. Godbey, M. Dasgupta, and D. J. Hinde, How the Pauli exclusion principle affects fusion of atomic nuclei, Phys. Rev. C **95**, 031601(R) (2017).
[12] C. H. Dasso and G. Pollarolo, Investigating the nucleus-nucleus potential at very short distances, Phys. Rev. C **68**, 054604 (2003).
[13] A. S. Umar, V. E. Oberacker, and C. J. Horowitz, Microscopic sub-barrier fusion calculations for the neutron star crust, Phys. Rev. C **85**, 055801 (2012).
[14] C. L. Jiang, H. Esbensen, K. E. Rehm, B. B. Back, R. V. F. Janssens, J. A. Caggiano, P. Collon, J. Greene, A. M. Heinz, D. J. Henderson, I. Nishinaka, T. O. Pennington, and D. Seweryniak, Unexpected Behavior of Heavy-Ion Fusion Cross Sections at Extreme Sub-Barrier Energies, Phys. Rev. Lett. **89**, 052701 (2002).
[15] M. Dasgupta, D. J. Hinde, A. Diaz-Torres, B. Bouriquet, C. I. Low, G. J. Milburn, and J. O. Newton, Beyond the Coherent Coupled Channels Description of Nuclear Fusion, Phys. Rev. Lett. **99**, 192701 (2007).
[16] A. M. Stefanini, G. Montagnoli, L. Corradi, S. Courtin, E. Fioretto, A. Goasduff, F. Haas, P. Mason, R. Silvestri, P. P. Singh, F. Scarlassara, and S. Szilner, Fusion hindrance for ^{58}Ni + ^{54}Fe, Phys. Rev. C **82**, 014614 (2010).
[17] B. B. Back, H. Esbensen, C. L. Jiang, and K. E. Rehm, Recent developments in heavy-ion fusion reactions, Rev. Mod. Phys. **86**, 317 (2014).
[18] T. Fliessbach, The optical potential for the elastic heavy ion scattering, Z. Phys. **247**, 117 (1971).
[19] D. M. Brink and F. Stancu, Interaction potential between two ^{16}O nuclei derived from the Skyrme interaction, Nucl. Phys. A **243**, 175 (1975).
[20] F. Beck, K.-H. Müller, and H. S. Köhler, Momentum Dependence of the Ion-Ion Potential in a Microscopic Theory, Phys. Rev. Lett. **40**, 837 (1978).
[21] B. Sinha and S. A. Moszkowski, The nucleus-nucleus interaction potential using density-dependent δ interaction, Phys. Lett. B **81**, 289 (1979).
[22] T. Fliessbach, The reduced width amplitude in the reaction theory for composite particles, Z. Phys. A **272**, 39 (1975).

[23] P. G. Zint and U. Mosel, Kinetic energy contributions to heavy ion potentials, Phys. Lett. B **56**, 424 (1975).

[24] D. M. Brink and F. Stancu, Microscopic and proximity nucleus-nucleus potentials, Nucl. Phys. A **299**, 321 (1978).

[25] V. Y. Denisov and V. A. Nesterov, Effect of the Pauli exclusion principle on the potential of nucleus-nucleus interaction, Phys. At. Nucl. **73**, 1142 (2010).

[26] K. Cheng and C. Xu, Pauli blocking effects in α-induced fusion reactions, Phys. Rev. C **99**, 014607 (2019).

[27] K. Cheng and C. Xu, Pauli blocking effects in $n\alpha$-nucleus-induced fusion reactions, Phys. Rev. C **102**, 014619 (2020).

[28] K. Aoki and H. Horiuchi, Study of local internucleus potential on the basis of the resonating group method. IV: Comparison of various approaches to calculate internucleus potential and study of the origins of deep and shallow potentials, Prog. Theor. Phys. **69**, 1154 (1983).

[29] T. Wada and H. Horiuchi, Comparison of the Microscopic Potential with the Optical Potential in the $\alpha + {}^{16}\mathrm{O}$ System, Phys. Rev. Lett. **58**, 2190 (1987).

[30] A. Tohsaki, F. Tanabe, and R. Tamagaki, Microscopic study of ${}^{16}\mathrm{O}$ - ${}^{16}\mathrm{O}$ interaction by the resonating group method, Prog. Theor. Phys. **53**, 1022 (1975).

[31] Y. C. Tang, M. LeMere, and D. R. Thompsom, Resonating-group method for nuclear many-body problems, Phys. Rep. **47**, 167 (1978).

[32] C. Simenel, Nuclear quantum many-body dynamics, Eur. Phys. J. A **48**, 152 (2012).

[33] C. Simenel and A. S. Umar, Heavy-ion collisions and fission dynamics with the time-dependent Hartree-Fock theory and its extensions, Prog. Part. Nucl. Phys. **103**, 19 (2018).

[34] P. D. Stevenson and M. C. Barton, Low-energy heavy-ion reactions and the Skyrme effective interaction, Prog. Part. Nucl. Phys. **104**, 142 (2019).

[35] K. Sekizawa, TDHF theory and its extensions for the multinucleon transfer reaction: A minireview, Front. Phys. **7**, 20 (2019).

[36] S. Levit, J. W. Negele, and Z. Paltiel, Barrier penetration and spontaneous fission in the time-dependent mean-field approximation, Phys. Rev. C **22**, 1979 (1980).

[37] H. Reinhardt, Semiclassical theory of nuclear fission, Nucl. Phys. A **367**, 269 (1981).

[38] P. Arve, G. F. Bertsch, J. W. Negele, and G. Puddu, Model for tunneling in many-particle systems, Phys. Rev. C **36**, 2018 (1987).

[39] P. McGlynn and C. Simenel, Imaginary-time mean-field method for collective tunneling, Phys. Rev. C **102**, 064614 (2020).

[40] K. Hagino and N. Takigawa, Subbarrier fusion reactions and many-particle quantum tunneling, Prog. Theor. Phys. **128**, 1001 (2012).

[41] V. A. Nesterov, Effect of the Pauli exclusion principle and the polarization of nuclei on the potential of their interaction for the example of the $^{16}\mathrm{O} + {}^{16}\mathrm{O}$ system, Phys. At. Nucl. **76**, 577 (2013).

[42] V. O. Nesterov, Influence of the Pauli exclusion principle and the polarization of nuclei on the nuclear part of the interaction potential in the $^{40}\mathrm{Ca} + {}^{40}\mathrm{Ca}$ system, Nucl. Phys. A **974**, 124 (2018).

[43] J. Skalski, Adiabatic fusion barriers from self-consistent calculations, Phys. Rev. C **76**, 044603 (2007).

[44] K. A. Brueckner, J. R. Buchler, and M. M. Kelly, New theoretical approach to nuclear heavy-ion scattering, Phys. Rev. **173**, 944 (1968).

[45] K. Hagino, N. Rowley, and A. T. Kruppa, A program for coupled-channel calculations with all order couplings for heavy-ion fusion reactions, Comput. Phys. Commun. **123**, 143 (1999).

[46] V. Y. Denisov and W. Nörenberg, Entrance channel potentials in the synthesis of the heaviest nuclei, Eur. Phys. J. A **15**, 375 (2002).

[47] K. Washiyama and D. Lacroix, Energy dependence of the nucleus-nucleus potential close to the Coulomb barrier, Phys. Rev. C **78**, 024610 (2008).

[48] C. Simenel and B. Avez, Time-dependent Hartree-Fock description of heavy ions fusion, Intl. J. Mod. Phys. E **17**, 31 (2008).

[49] L. Guo and T. Nakatsukasa, Time-dependent Hartree-Fock studies of the dynamical fusion threshold, EPJ Web Conf. **38**, 09003 (2012).

[50] K. Vo-Phuoc, C. Simenel, and E. C. Simpson, Dynamical effects in fusion with exotic nuclei, Phys. Rev. C **94**, 024612 (2016).

[51] C. Simenel, M. Dasgupta, D. J. Hinde, and E. Williams, Microscopic approach to coupled-channels effects on fusion, Phys. Rev. C **88**, 064604 (2013).

[52] A. S. Umar and V. E. Oberacker, Heavy-ion interaction potential deduced from density-constrained time-dependent Hartree-Fock calculation, Phys. Rev. C **74**, 021601(R) (2006).

[53] A. D. Becke and K. E. Edgecombe, A simple measure of electron localization in atomic and molecular systems, J. Chem. Phys. **92**, 5397 (1990).

[54] T. Burnus, M. A. L. Marques, and E. K. U. Gross, Time-dependent electron localization function, Phys. Rev. A **71**, 010501(R) (2005).

[55] A. Savin, The electron localization function (ELF) and its relatives: Interpretations and difficulties, J. Mol. Struct. Theochem. **727**, 127 (2005).

[56] P. Jerabek, B. Schuetrumpf, P. Schwerdtfeger, and W. Nazarewicz, Electron and Nucleon Localization Functions of Oganesson: Approaching the Thomas-Fermi Limit, Phys. Rev. Lett. **120**, 053001 (2018).

[57] P.-G. Reinhard, J. A. Maruhn, A. S. Umar, and V. E. Oberacker, Localization in light nuclei, Phys. Rev. C **83**, 034312 (2011).

[58] J.-P. Ebran, E. Khan, T. Nikšić, and D. Vretenar, Localization and clustering in atomic nuclei, J. Phys. G **44**, 103001 (2017).

[59] B. Schuetrumpf and W. Nazarewicz, Cluster formation in precompound nuclei in the time-dependent framework, Phys. Rev. C **96**, 064608 (2017).

[60] C. L. Zhang, B. Schuetrumpf, and W. Nazarewicz, Nucleon localization and fragment formation in nuclear fission, Phys. Rev. C **94**, 064323 (2016).

[61] G. Scamps and C. Simenel, Impact of pear-shaped fission fragments on mass-asymmetric fission in actinides, Nature (London) **564**, 382 (2018).

[62] G. Scamps and C. Simenel, Effect of shell structure on the fission of sub-lead nuclei, Phys. Rev. C **100**, 041602(R) (2019).

[63] Z. Matheson, S. A. Giuliani, W. Nazarewicz, J. Sadhukhan, and N. Schunck, Cluster radioactivity of $^{290}_{117}\mathrm{Og}_{176}$, Phys. Rev. C **99**, 041304(R) (2019).

[64] J. Sadhukhan, S. A. Giuliani, Z. Matheson, and W. Nazarewicz, Efficient method for estimation of fission fragment yields of *r*-process nuclei, Phys. Rev. C **101**, 065803 (2020).

[65] T. Li, M. Z. Chen, C. L. Zhang, W. Nazarewicz, and M. Kortelainen, Nucleon localization function in rotating nuclei, Phys. Rev. C **102**, 044305 (2020).

[66] T. H. R. Skyrme, CVII. The nuclear surface, Phil. Mag. **1**, 1043 (1956).

[67] J. Fleckner and U. Mosel, Antisymmetrization effects in heavy ion potentials, Nucl. Phys. A **277**, 170 (1977).

[68] H. Flocard and M. S. Weiss, Generation of high-frequency components in TDHF heavy-ion collisions, Phys. Lett. B **105**, 14 (1981).

[69] C. Simenel, R. Keser, A. S. Umar, and V. E. Oberacker, Microscopic study of $^{16}O + ^{16}O$ fusion, Phys. Rev. C **88**, 024617 (2013).

[70] C. Simenel, P. Chomaz, and G. de France, Quantum Calculations of Coulomb Reorientation for Sub-Barrier Fusion, Phys. Rev. Lett. **93**, 102701 (2004).

[71] A. S. Umar and V. E. Oberacker, Time-dependent Hartree-Fock fusion calculations for spherical, deformed systems, Phys. Rev. C **74**, 024606 (2006).

[72] A. S. Umar, V. E. Oberacker, and J. A. Maruhn, Neutron transfer dynamics and doorway to fusion in time-dependent Hartree-Fock theory, Eur. Phys. J. A **37**, 245 (2008).

[73] C. Simenel, Particle Transfer Reactions with the Time-Dependent Hartree-Fock Theory Using a Particle Number Projection Technique, Phys. Rev. Lett. **105**, 192701 (2010).

[74] K. Sekizawa and K. Yabana, Time-dependent Hartree-Fock calculations for multinucleon transfer processes in $^{40,48}Ca + ^{124}Sn$, $^{40}Ca + ^{208}Pb$, and $^{58}Ni + ^{208}Pb$ reactions, Phys. Rev. C **88**, 014614 (2013).

[75] K. Godbey, A. S. Umar, and C. Simenel, Dependence of fusion on isospin dynamics, Phys. Rev. C **95**, 011601(R) (2017).

[76] X. Jiang and N. Wang, Probing the production mechanism of neutron-rich nuclei in multinucleon transfer reactions, Phys. Rev. C **101**, 014604 (2020).

[77] K. Washiyama and K. Sekizawa, TDHF and a macroscopic aspect of low-energy nuclear reactions, Front. Phys. **8**, 93 (2020).

[78] A. S. Umar, V. E. Oberacker, J. A. Maruhn, and P.-G. Reinhard, Microscopic composition of ion-ion interaction potentials, Phys. Rev. C **85**, 017602 (2012).

[79] A. S. Umar, V. E. Oberacker, J. A. Maruhn, and P.-G. Reinhard, Microscopic calculation of precompound excitation energies for heavy-ion collisions, Phys. Rev. C **80**, 041601(R) (2009).

[80] R. Keser, A. S. Umar, and V. E. Oberacker, Microscopic study of Ca + Ca fusion, Phys. Rev. C **85**, 044606 (2012).

[81] A. S. Umar, C. Simenel, and V. E. Oberacker, Energy dependence of potential barriers and its effect on fusion cross sections, Phys. Rev. C **89**, 034611 (2014).

[82] A. S. Umar and V. E. Oberacker, Density-constrained time-dependent Hartree-Fock calculation of $^{16}O + ^{208}Pb$ fusion cross-sections, Eur. Phys. J. A **39**, 243 (2009).

[83] V. E. Oberacker and A. S. Umar, Microscopic analysis of sub-barrier fusion enhancement in $^{132}Sn + ^{40}Ca$ versus $^{132}Sn + ^{48}Ca$, Phys. Rev. C **87**, 034611 (2013).

[84] X. Jiang, J. A. Maruhn, and S. Yan, Microscopic study of noncentral effects in heavy-ion fusion reactions with spherical nuclei, Phys. Rev. C **90**, 064618 (2014).

[85] L. Guo, C. Simenel, L. Shi, and C. Yu, The role of tensor force in heavy-ion fusion dynamics, Phys. Lett. B **782**, 401 (2018).

[86] L. Guo, K. Godbey, and A. S. Umar, Influence of the tensor force on the microscopic heavy-ion interaction potential, Phys. Rev. C **98**, 064607 (2018).

[87] G. Scamps and Y. Hashimoto, Density-constrained time-dependent Hartree-Fock-Bogoliubov method, Phys. Rev. C **100**, 024623 (2019).

[88] K. Godbey, C. Simenel, and A. S. Umar, Absence of hindrance in microscopic $^{12}C + ^{12}C$ fusion study, Phys. Rev. C **100**, 024619 (2019).

[89] Y. M. Engel, D. M. Brink, K. Goeke, S. J. Krieger, and D. Vautherin, Time-dependent Hartree-Fock theory with Skyrme's interaction, Nucl. Phys. A **249**, 215 (1975).

[90] M. Bender, P.-H. Heenen, and P.-G. Reinhard, Self-consistent mean-field models for nuclear structure, Rev. Mod. Phys. **75**, 121 (2003).

[91] E. Perlińska, S. G. Rohoziński, J. Dobaczewski, and W. Nazarewicz, Local density approximation for proton-neutron pairing correlations: Formalism, Phys. Rev. C **69**, 014316 (2004).

[92] S. Pittalis, E. Räsänen, and C. R. Proetto, Becke-Johnson-type exchange potential for two-dimensional systems, Phys. Rev. B **81**, 115108 (2010).

[93] C. F. von Weizsäcker, Zur Theorie der Kernmassen, Z. Phys. A **96**, 431 (1935).

[94] A. S. Umar and V. E. Oberacker, Three-dimensional unrestricted time-dependent Hartree-Fock fusion calculations using the full Skyrme interaction, Phys. Rev. C **73**, 054607 (2006).

[95] K.-H. Kim, T. Otsuka, and P. Bonche, Three-dimensional TDHF calculations for reactions of unstable nuclei, J. Phys. G: Nucl. Part. Phys. **23**, 1267 (1997).

[96] C. Bottcher, M. R. Strayer, A. S. Umar, and P.-G. Reinhard, Damped relaxation techniques to calculate relativistic bound states, Phys. Rev. A **40**, 4182 (1989).

[97] A. S. Umar, M. R. Strayer, J. S. Wu, D. J. Dean, and M. C. Güçlü, Nuclear Hartree-Fock calculations with splines, Phys. Rev. C **44**, 2512 (1991).

[98] A. S. Umar, J. Wu, M. R. Strayer, and C. Bottcher, Basis-spline collocation method for the lattice solution of boundary-value-problems, J. Comp. Phys. **93**, 426 (1991).

[99] V. I. Zagrebaev, Synthesis of superheavy nuclei: Nucleon collectivization as a mechanism for compound nucleus formation, Phys. Rev. C **64**, 034606 (2001).

[100] C. Simenel, K. Godbey, and A. S. Umar, Timescales of Quantum Equilibration, Dissipation, and Fluctuation in Nuclear Collisions, Phys. Rev. Lett. **124**, 212504 (2020).

[101] M. Evers, M. Dasgupta, D. J. Hinde, D. H. Luong, R. Rafiei, R. du Rietz, and C. Simenel, Cluster transfer in the reaction $^{16}O + ^{208}Pb$ at energies well below the fusion barrier: A possible doorway to energy dissipation, Phys. Rev. C **84**, 054614 (2011).

[102] D. C. Rafferty, M. Dasgupta, D. J. Hinde, C. Simenel, E. C. Simpson, E. Williams, I. P. Carter, K. J. Cook, D. H. Luong, S. D. McNeil, K. Ramachandran, K. Vo-Phuoc, and A. Wakhle, Multinucleon transfer in $^{16,18}O$, $^{19}F + ^{208}Pb$ reactions

at energies near the fusion barrier, Phys. Rev. C **94**, 024607 (2016).

[103] Ş. Mişicu and H. Esbensen, Hindrance of Heavy-Ion Fusion Due to Nuclear Incompressibility, Phys. Rev. Lett. **96**, 112701 (2006).

[104] A. M. Stefanini, G. Montagnoli, H. Esbensen, P. Čolović, L. Corradi, E. Fioretto, F. Galtarossa, A. Goasduff, J. Grebosz, F. Haas, M. Mazzocco, N. Soić, E. Strano, and S. Szilner, New results in low-energy fusion of ^{40}Ca + ^{90,92}Zr, Phys. Rev. C **96**, 014603 (2017).

[105] A. M. Stefanini, G. Montagnoli, M. Del Fabbro, G. Colucci, P. Čolović, L. Corradi, E. Fioretto, F. Galtarossa, A. Goasduff, J. Grebosz, M. Heine, G. Jaworski, M. Mazzocco, T. Mijatovic, S. Szilner, M. Bajzek, D. Brugnara, M. Siciliano, and I. Zanon, Fusion hindrance and Pauli blocking in ^{58}Ni + ^{64}Ni, Phys. Rev. C **100**, 044619 (2019).